Translational Oncology 27 (2023) 101584

Contents lists available at ScienceDirect

Translational Oncology

journal homepage: www.elsevier.com/locate/tranon

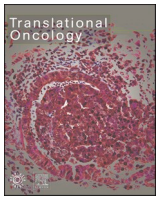

Synthesis and optimization of photothermal properties of NIR emitting $LiGa_5O_8$: Cr^{3+} and gold nanorods as hybrid materials for theranostic applications

C. Belman-Rodriguez [a,b,*], Prakhar Sengar [b], Gustavo A. Hirata [b], Joaquin Manzo-Merino [c], Marcela Lizano [d,e], Mario H. Farías [b], Sergio A. Aguila [b,*]

[a] Posgrado en Física de Materiales, Centro de Investigación Científica y de Educación Superior de Ensenada, Carretera Tijuana-Ensenada No. 3918, Zona Playitas, Ensenada, Baja California 22860, México
[b] Centro de Nanociencias y Nanotecnología, Universidad Nacional Autónoma de México, AP 14, Ensenada, Baja California 22860, México
[c] Cátedras CONACyT-Instituto Nacional de Cancerología, México City 14080, México
[d] Unidad de Investigación Biomédica en Cáncer, Instituto Nacional de Cancerología-Instituto de Investigaciones Biomédicas, Universidad Nacional Autónoma de México, Mexico City 14080, Mexico
[e] Departamento de Medicina Genómica y Toxicología Ambiental, Instituto de Investigaciones Biomédicas, Universidad Nacional Autónoma de México, Ciudad Universitaria, Mexico City 04510, Mexico

ARTICLE INFO

Keywords:
Hybrid materials
LGO
Near infrared
AuR

ABSTRACT

The increase in incidence of degenerative diseases has fueled the development of novel materials, mostly focused on reducing adverse effects caused by current medical therapies. Theranostic materials represent an alternative to treat degenerative diseases, since they combine diagnostic properties and localized therapy within the same material. This work presents the synthesis and characterization of hybrid materials designed for theranostic purposes. The hybrid materials were composed of $LiGa_5O_8$:Cr^{3+} (LGO) with emission lines in the near infrared (NIR), hence providing an excellent diagnostic ability. As for the therapy part, the hybrid nanomaterials contained gold nanorods (AuR) with localized surface plasmon resonance (LSPR). Once AuR are excited, plasmonic processes are triggered at their surface resulting in increased localized temperature capable of inducing irreversible damage to the cells. A detailed characterization of the hybrid materials confirmed proper assembly of LGO and AuR. Moreover, these nanocomposites preserved their luminescent properties and LSPR. Finally, the cytotoxic potential of the hybrid material was evaluated in different cell lines by cell viability colorimetric assays to determine its possible use as theranostic agent. The success in the synthesis of hybrid materials based on LGO with emission in the NIR coupled with AuR, provides a new perspective for the design of hybrid materials with improved properties to be used in biomedical fields.

Introduction

Research in nanomedicine has turned to the study and development of nanomaterials for diagnosis and treatment of diseases such as cancer. Advances lie in the physicochemical modifications of nanomaterials aimed to change their morphology and surface properties to improve their biodistribution and optimize them for specific biomedical applications [1–3]. For example, biotracers have been developed from luminescent materials to monitor pathogenic organisms in biological systems. To provide specificity to biotracers, the nanoparticle surface has been functionalized with ligands [4].

The development of new luminescent materials with emission within the first biological window (650–1000 nm) has drawn extensive attention in the biological and the medical fields [5]. NIR light shows lower absorption by hemoglobin and scattering by biomolecules present in the human tissue compared to UV or visible light, resulting in increased transparency of biological tissue towards NIR light [6].

LGO is a luminescent material used as a biotracer, which presents emission lines within the NIR. Furthermore, LGO also has radioluminescent properties; that is, the luminescent processes can be activated with high-energy light irradiation. This light is also capable of crossing tissues and activating the emission process. This is a practical

* Corresponding authors.
E-mail addresses: belman25@ens.cnyn.unam.mx (C. Belman-Rodriguez), aguila@ens.cnyn.unam.mx (S.A. Aguila).

https://doi.org/10.1016/j.tranon.2022.101584
Received 4 May 2022; Received in revised form 29 June 2022; Accepted 3 November 2022

technique commonly used in disease detection [7–9].

On the other hand, metallic nanoparticles have been evaluated as new therapeutic agents against several degenerative diseases, including cancer. Among the main characteristics of metallic nanoparticles are the display of the photophysical phenomenon LSPR, and their inherently low toxicity. The plasmonic properties of nanoparticles can be used for plasmonic photothermal therapy (PPTT) in which photon energy is converted into sufficient heat to destroy cancer cells [10–12].

Noble metal nanoparticles provide remarkable opportunities for biomedical applications due to their inherent low toxicity [3,11]. Au nanoparticles have been amply studied for use in PPTT. Crucially, by changing their structure and shape, the LSPR frequency of gold nanoparticles can be tuned in order to fit into the NIR region [12]. Due to the minimal attenuation by water and hemoglobin at these wavelengths, NIR may be transmitted in soft tissues to depths exceeding 10 cm [11]. Moreover, gold nanorods (AuR) have been described as the most effective photothermal contrast agent for *in vivo* and *in vitro* treatments [10].

In recent years, hybrid nanomaterials based on organic-inorganic resources have been developed by combining different nanostructured materials, merging their individual properties with the aim of improving them. These nanosystems can be prepared using nanocomponents endowed with diagnostic and therapeutic functions, adhering to the concept of a "theranostic" device. Administration of these nanosystems would provide diagnostic and therapeutic procedures in a single dose [13].

Herein we report the synthesis and characterization of NIR-emitting LGO with AuR of different aspect ratio coupled onto the surface of LGO by means of chemical conjugation. The chemical method to obtain the hybrid material was based on organic-inorganic interactions, which involved the coupling of two inorganic phases (LGO and AuR), using (3-mercaptopropyl) trimethoxysilane (MPTMS) and (3-aminopropyl) trimethoxysilane (AMPTMS) sulfonates as organic spacers. The purpose of this coupling was to improve the emission properties of the LGO nanocrystal in the NIR, as a potential diagnostic agent. Moreover, the presence of AuR on LGO nanocrystals can provide LSPR ability, which is associated with an increase in temperature that could damage a variety of cells irreversibly. We also optimized the LSPR properties of the hybrid nanosystem by varying the aspect ratio of the coupled AuR.

Preliminary results demonstrate the capacity of the hybrid system to emit NIR photons and to display a photothermal effect upon NIR (800 nm) excitation. Additionally, the cytotoxic effect of the hybrid materials was evaluated by *in vitro* assays in various cell lines.

Experimental

Materials

$LiGa_2O_8:Cr^{3+}$ was synthesized by the sol-gel method using lithium nitrate ($LiNO_3$ 99.99% Sigma Aldrich), gallium nitrate ($Ga(NO_3)_3$, 99.99%, Sigma Aldrich) and chromium nitrate ($Cr(NO_3)_3$, 99.99%, Sigma Aldrich) as precursors. L(+)-tartaric acid ($C_4H_6O_6$, 99.5%, Sigma Aldrich) was used as the chelating agent for the polymeric precursor method.

Synthesis of $LiGa_5O_8:Cr^{3+}$ (LGO)

The LGO phosphor was synthesized by the tartaric acid-assisted sol-gel method [14,15]. All chemicals used were analytical grade reagents without further purification. The precursor nitrates were used in stoichiometric proportions to obtain LGO doped with 1% of Cr^{3+}. $LiNO_3$, $Ga(NO_3)_3$ and $Cr(NO_3)_3$ were dissolved in 25 mL deionized water and the mixture was stirred for 24 h at room temperature. Then, the mixture was heated to 80 °C for 2 h. Thereafter, the solution was heated to 120 °C until dry to form a xerogel. Finally, the xerogel was annealed at 1100 °C for 3 h with heating rate of 5 °C/min.

Table 1
Summary of the synthesis process of the hybrid material based on LGO.

Conjugates LGO@SiO2 1 mL	+	AuR14 450 μL	AuR18 300 μL	AuR20 150 μL 600 μL
Sample label		L@450D14	L@300D18	L@150D20 L@600D20

Synthesis of Au nanorods (AuR)

A seed-mediated method was used to prepare AuR with three different aspect ratios. Two steps were typically included, as Nikoobakht and El-Sayed reported [16]. First, the gold seeds were synthesized, and then AuR was synthesized with three different aspect ratios, varying the amount of seed in the growth solution.

Seed solution. CTAB solution (5 mL, 0.1 M) was mixed with 12.5 μL of 0.25 mM $HAuCl_4$. To the stirred solution, 0.3 mL of cold 0.02 M $NaBH_4$ was added. The stirring of seed solution was continued for 20 min.

Growth of AuR. Three different growth solutions were prepared to obtain AuR with different aspect ratios. Each solution was prepared as follows: CTAB solution (10 mL, 0.1 M) was mixed under vigorous stirring with 0.5 mL of 10 mM $HAuCl_4$, 24 μL of 50 mM $AgNO_3$, 80 μL of 0.8 mM ascorbic acid, 0.186 mL of 0.5 mM HCl specifically in this order. In the last step, the three AuR solutions were prepared by adding 14, 18, and 20 μL of seed to obtain three samples, which were named AuR14, AuR18 and AuR20, in conformity with the amount of seed that was added to each sample. All samples contained 0.1 M CTAB concentration.

Synthesis of the hybrid material ($LiGa_5O_8:Cr^{3+}@SiO_2$-AuR)

$LiGa_5O_8:Cr^{3+}@SiO_2$ (LGO@SiO_2) was conjugated with AuR as described in previous work [17]. A total of 20 mg of LGO@SiO_2 were suspended in 30 mL of ethanol, then 15 μL of (3-mercaptopropyl) trimethoxysilane (MPTMS) and 5 μL (3-aminopropyl) trimethoxysilane (AMPTMS) were added to the mixture of LGO@SiO_2 and stirred for 12 h at room temperature. After 12 h, the above mixture was heated to 70 °C for 1 h and some aliquots were added to maintain a constant volume of ethanol. The mixture was washed 3 times by centrifugation at 5500 rpm and the supernatant removed. After washing, the samples were resuspended in 30 mL of ethanol to obtain a stock solution. The AuR samples (AuR14, AuR18 and AuR20) were prepared to reduce the CTAB concentration from 0.1M to 1 mM.

To conjugate both materials, microtubes were prepared with 1 mL of the stock solution. Then, different amounts of AuR with CTAB (1 Mm) were added as follows: 150 μL of AuR20, 300 μL of AuR18, 450 μL of AuR14 and 600 μL of AuR20, respectively. The 4 tubes were placed under stirring for 2 h and centrifuged 3 times at 800 rpm, and subsequently resuspended in ethanol to eliminate the remnants of AuR in the synthesis. Finally, 4 samples of hybrid materials were prepared: LGO@SiO_2-150AuR20 was labeled (L@150D20); LGO@SiO_2-300AuR18, (L@300D18); LGO@SiO_2-450AuR14, (L@450D14); and LGO@SiO_2-600AuR20, (L@600D20). Table 1 summarizes the reagents used during the synthesis.

Assays of temperature increase

Based on the report by Mackey et al. [10], the hybrid materials were irradiated with an 808 nm wavelength laser, and an optical heater was designed. A laser with an output power between 0.4 and 1.6 W was used. The laser output was regulated with an Instek GDP-4303S power source. A quartz sample holder with a volume of 0.7 mL was used. A type T thermocouple with a diameter of 0.2 mm and a response error of ±0.2 °C was used to measure the temperature.

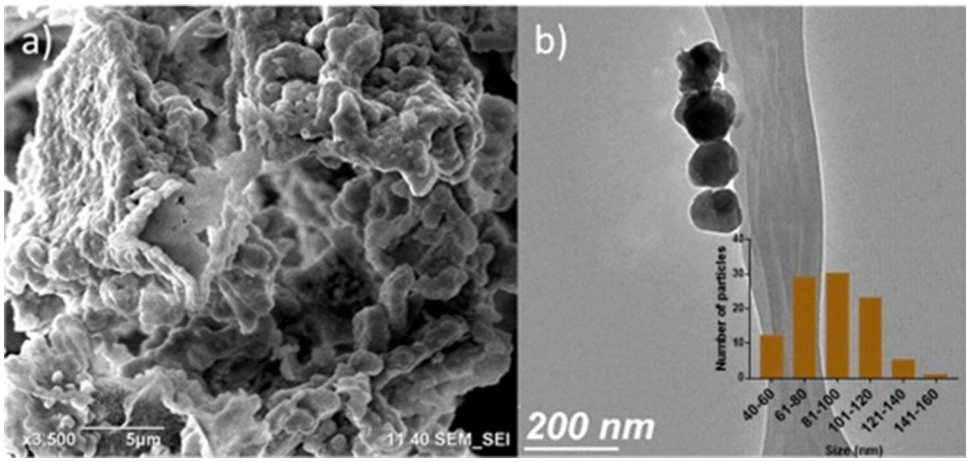

Fig. 1. SEM (a) and TEM (b) images of synthetized LGO.

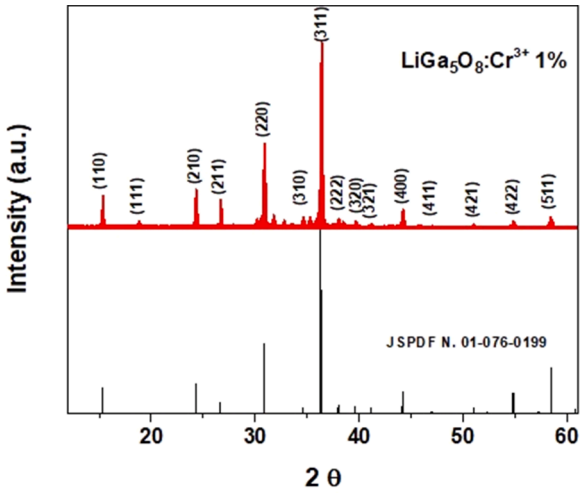

Fig. 2. XRD patterns of LGO samples obtained by the polymeric precursor method synthesis assisted by tartaric acid.

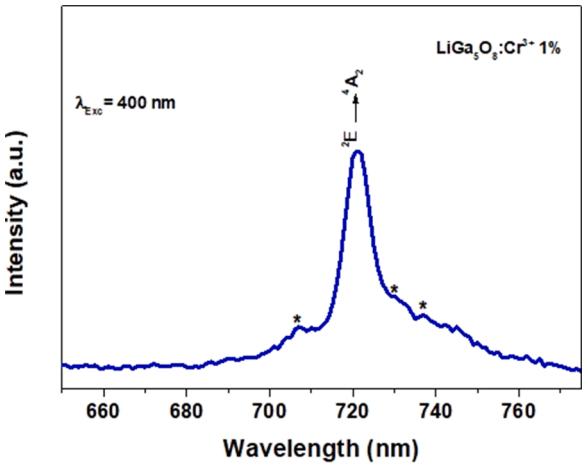

Fig. 3. Photoluminescence emission spectra of LGO, obtained with an excitation wavelength of 400 nm.

Cell viability assay

The cytotoxic effect of the hybrid materials was evaluated in *in vitro* assays with different cell lines, including HeLa (derived from cervical cancer) and NCI-H1299 (derived from epithelial lung cancer) obtained from ATCC. Also, cell viability was assessed in the normal immortalized keratinocytes cell line HaCaT, provided by the *Instituto Nacional de Cancerología*, México. Cells were maintained in Dubelccoś Modified Eagleś Medium (DMEM) with 10% fetal bovine serum (FBS) at 37° in humified CO_2 atmosphere. Cell viability was assessed using the colorimetric assay based on the reduction by mitochondrial dehydrogenase enzymes of the 3-(4,5-dimethylthiazol-2-yl)-5-(3-carboxymethoxyphenyl)-2-(4-sulfophenyl)-2H-tetrazolium (MTS) salt to blue formazan crystals.

The hybrid materials were diluted in DMEM to 0.0001, 0.001, 0.01, 0.1 and 1.0 µg. Cells were exposed to each concentration for 24 h in a 96-well plate containing 10,000 cells per well. Treated cells were incubated, and cell viability was tested with the *in vitro* cell proliferation assay Celltiter 96 (Promega) according to the manufacturerś instructions. Then, absorbance was measured using an ELISA plate reader (Thermo Scientific) at 490 nm. Obtained data were normalized and graphed. Cell lines without treatment were used as negative control. An analysis of variance was performed, considering a p value of 0.05 as statically significant.

Results and discussion

Results of LGO

LGO materials were synthesized by the tartaric acid-assisted sol-gel method and analyzed by means of scanning electron microscopy (SEM), transmission electron microscopy (TEM), X-ray diffraction (XRD), and photoluminescence spectroscopy (PL).

The SEM and TEM analyzes of LGO revealed the morphology and microstructure of the obtained materials. SEM micrographs showed that particles produce nanoparticle clusters (Fig. 1a), as reported in previous studies [8]. TEM images revealed that LGO nanoparticles are semi-spherical in morphology and have a particle size of ~93 nm (Fig. 1b). These results could be determining for biomedical applications due to the smaller particle size which in turn could allow a good biodistribution, an essential feature required for possible biomedical applications [18].

The diffraction peaks of the as synthesized LGO samples was indexed in agreement with the ICSD card N. 76-199 (Fig. 2). The synthesized LGO samples were crystalline with a typical spinel phase of $LiGa_5O_8$ [8]. The reference pattern corresponds to a crystal with space group $P4_332$, which derives from the Fd3m space group of spinel crystals [19]. The diffractogram does not show any secondary phase associated with the presence of impurities.

Photoluminescence spectroscopies were performed to confirm the

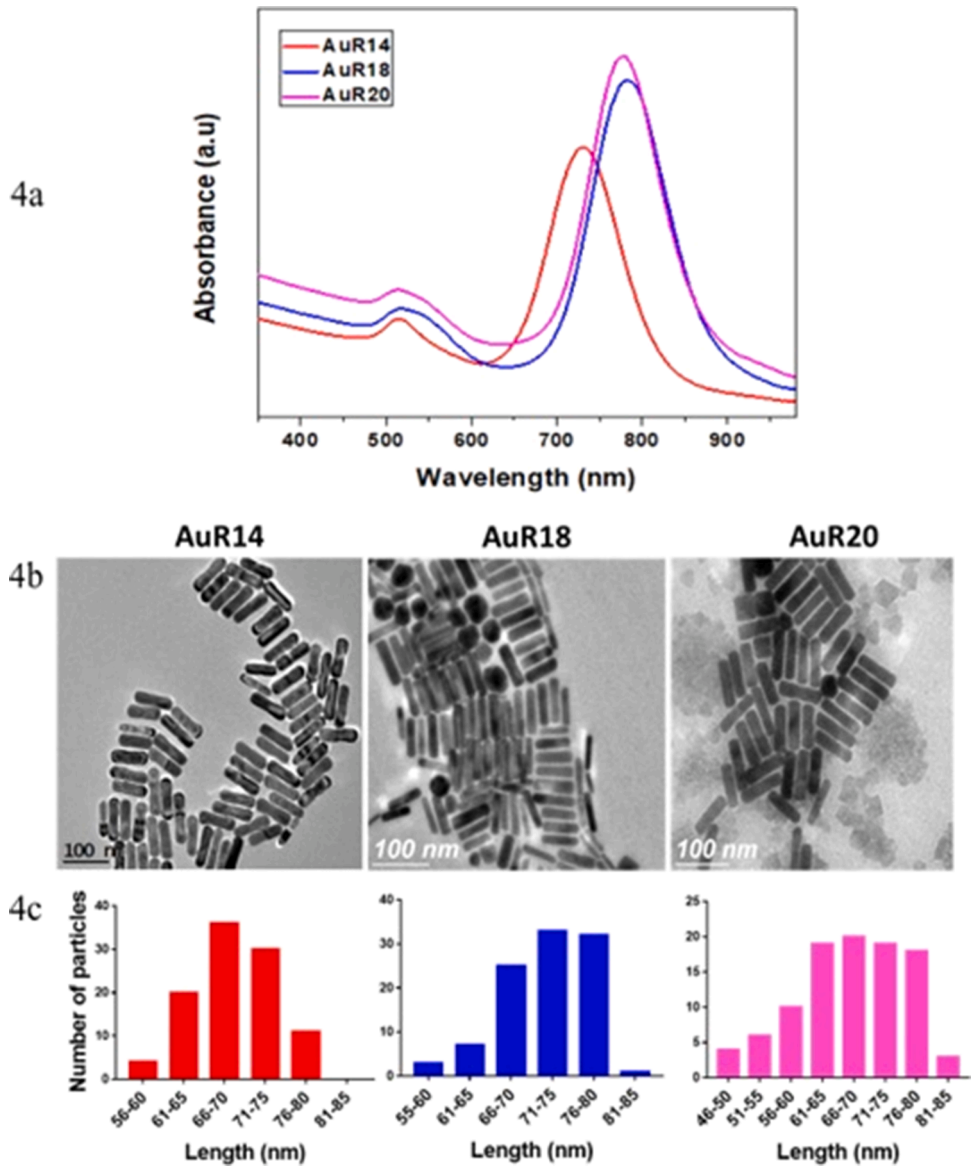

Fig. 4. (a) Absorbance graphs obtained by Uv-Vis for AuR synthesized by seed-mediated method. The charts were obtained when 14, 18, and 20 μL of seeds were added to the synthesis in each assay. (b) TEM micrographs of the different AuR. (c) AuR particle size distribution histograms.

presence of Cr^{3+} ion in the LGO lattice. Fig. 3 shows the PL emission spectrum, with a sharp line centered at 720 nm when excited with 400 nm, which corresponds to the zero-phonon emission of Cr^{3+} from the ^2E state to the $^4A_2$ ground state. The emission was accompanied by stokes and anti-stokes phonon sidebands at 706, 729 and 737 nm (*), typical of the Cr^{3+} ion in the lattice of LGO [9]. Taken together, these results indicate that the LGO synthesis by sol-gel was successful. The LGO results match those reported in the literature [9].

Results of gold nanorods (AuR)

The LSPR of AuR was determined by means of UV-Vis analysis. Fig. 4a shows 3 different spectra, corresponding to the AuR14, AuR18 and AuR20 samples. Each graph presents 2 peaks, the first centered at ~540 nm corresponding to transverse LSPR [20]. The second signal centered at ~730 nm for AuR14, at ~777 nm for AuR18, and at ~783 nm for AuR20 corresponds to longitudinal LSPR [20]. The absorption wavelength corresponding to the longitudinal LSPR is critical, as upon excitation with this wavelength the LSPR is activated leading to the localized heating of the AuR.

The morphology and the average size of the AuR were analyzed by TEM. Fig. 4b shows the typical morphology of AuR in the 3 different samples. To calculate the aspect ratio average of each sample, an analysis was performed. The results of aspect ratio were ~3.2, ~3.1 and ~3.5 for the AuR14, AuR18, and AuR20, respectively. The longitudinal size distribution for each sample of AuR is shown in Fig. 4c, where the AuR14 presents rods with length between 66 and 75 nm, the AuR18 between 66 and 75 nm, and the AuR20 between 61 and 80 nm. Although the range of lengths is similar, the small difference between them allows the variation of the absorbance by each sample.

Characterization of hybrid materials

The hybrid materials were characterized by SEM. Micrographs show white spots (red circle) attributed to the presence of AuR on the LGO surface, and the successful anchoring of the AuR mediated by MPTMS-AMPTMS with the ratios described in section 2 (Fig. 5). Fig. 5 also shows that the white clusters associated with the presence of AuR, apparently do not present agglomerations. The observed larger white particles, where the AuR is deposited, are associated with the LGO

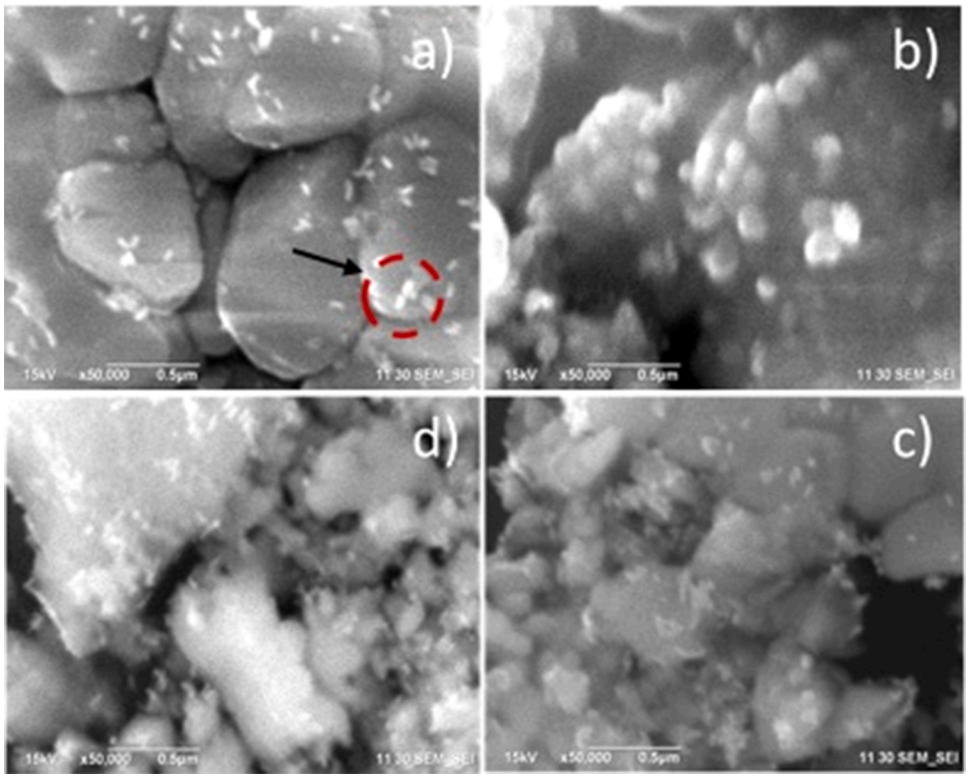

Fig. 5. Topographic images of the hybrid materials acquired by SEM: (a) L@SiO_2-450D14, (b) L@SiO_2-300D18, (c) L@SiO_2-150D20 (d) L@SiO_2-600D20.

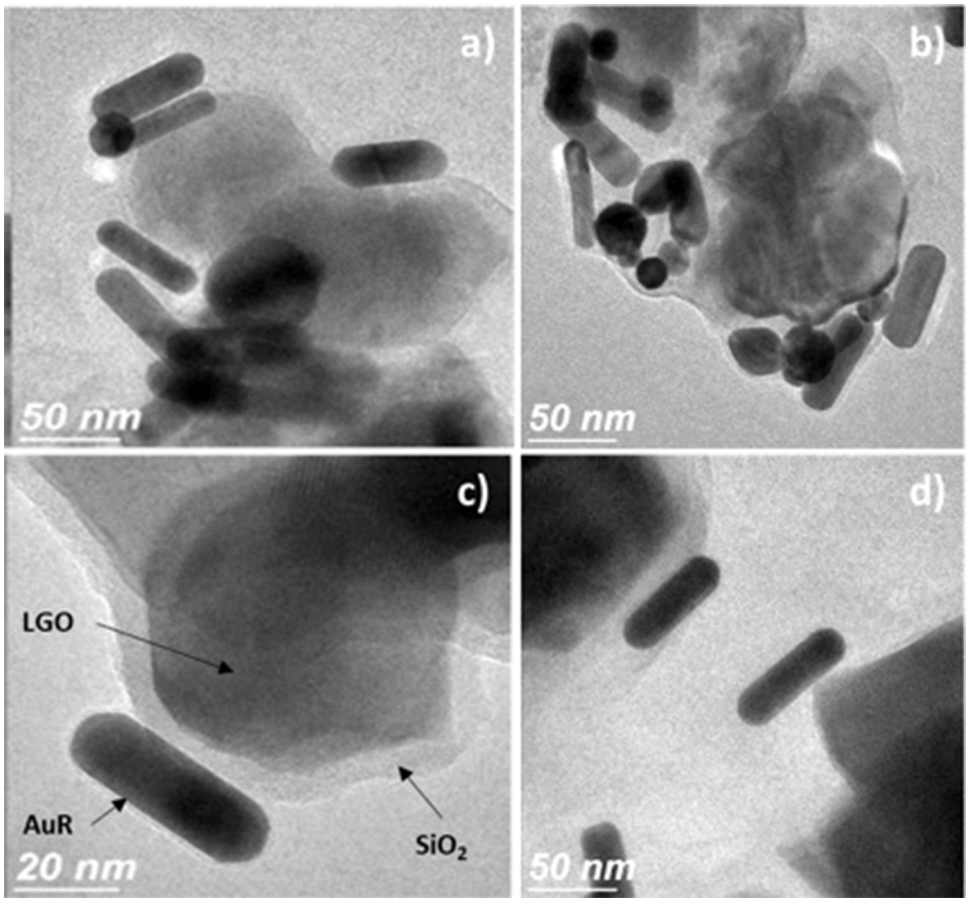

Fig. 6. TEM images: (a) L@SiO_2-450D14, (b) L@SiO_2-300D18, (c) L@SiO_2-150D20 (d) L@SiO_2-600D20

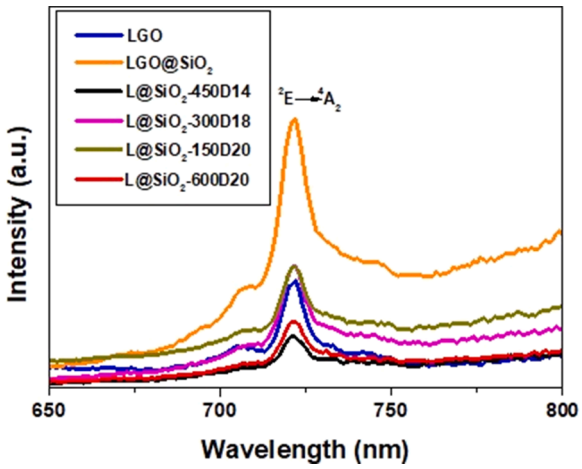

Fig. 7. Photoluminescence emission spectra obtained of the hybrid materials based on LGO. The measurement was performed at 400 nm excitation wavelength.

surface.

The morphology of the hybrid materials was also analyzed by TEM (Fig. 6). The micrographs show a hybrid material composed of a nucleus of luminescent properties (LGO), coated with silica, which interacts chemically with AuR. In this material, the silica coating has a homogeneous thickness of ~10 nm. It is important to notice that the silica coating led to the encapsulation of more than one nanoparticle, thus increasing the nanoparticle size of the hybrid materials to ~210 nm. Despite the variation of AuR amount in each sample, the TEM micrographs do not show apparently large differences in the amount of surface-anchored AuR between the different samples.

The TEM characterization revealed the successful synthesis of the hybrid materials. However, one of the most critical points was preserving the physicochemical characteristics that LGO and AuR can confer to hybrid materials.

The luminescent properties of the hybrid materials were analyzed by PL (Fig. 7). All samples exhibit the presence of an emission peak centered at ~720 nm when excited with 400 nm. The emission corresponds to the presence of the LGO in the core of the hybrid materials, and is associated with the $^2E \rightarrow {}^4A_2$ radiative transition of the Cr^{3+} ion [7]. The strongest peak emission is presented for the LGO sample, while hybrid materials show attenuation of the same peak. This phenomenon can be attributed to the non-radiative components of hybrid materials, such as the AuR present on their surface.

PL characterization revealed no shift with an emission centered in the infrared region associated with the $^2E \rightarrow {}^4A_2$ signal. Thus, the luminescent properties were maintained by the hybrid materials, giving them the property of emitting in the first biological window, which is adequate to satisfy their diagnostic function in future biomedical applications.

The hybrid materials were characterized by UV-Vis to determine the

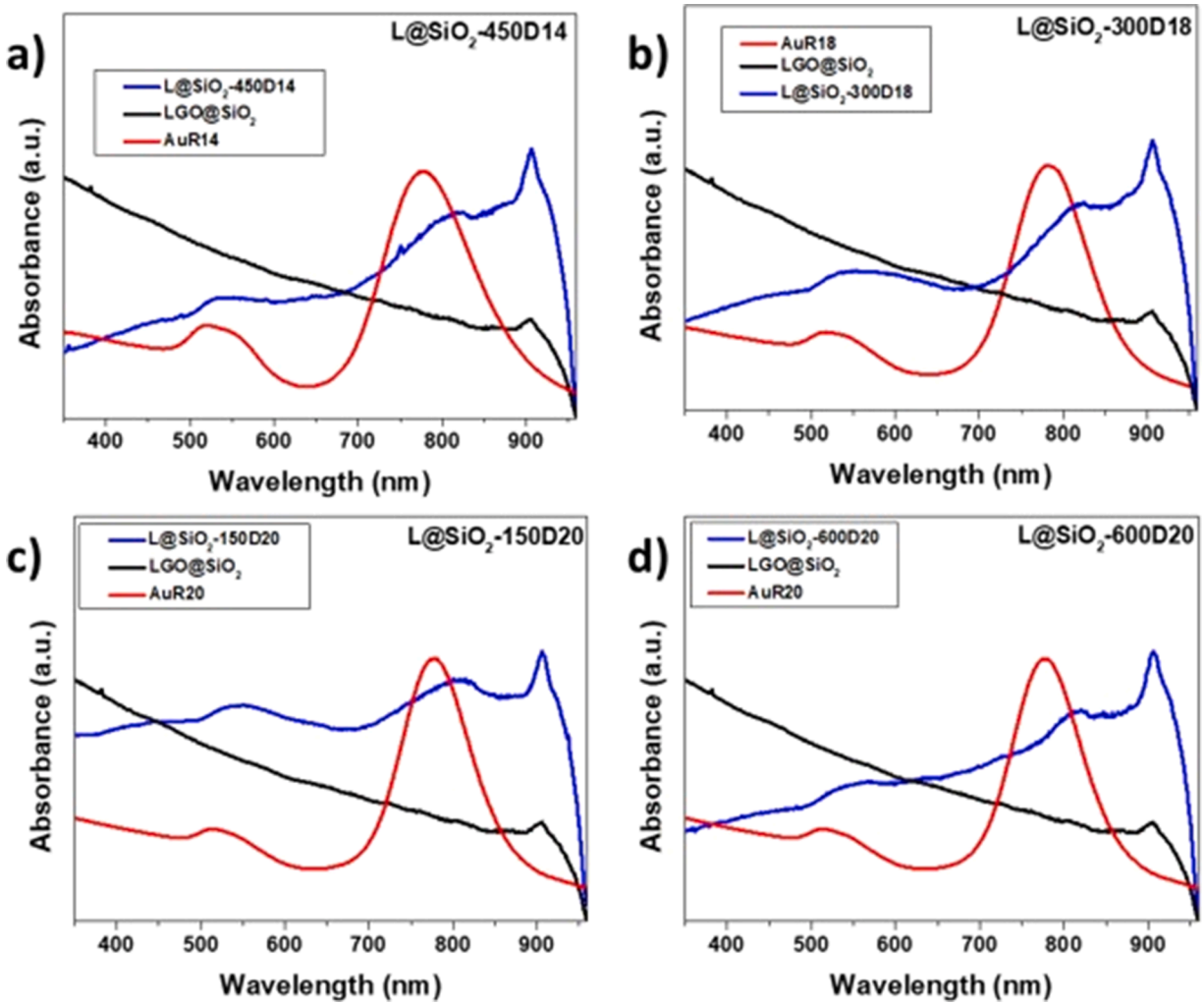

Fig. 8. Optical absorption (Uv-Vis): (a) LGO@SiO_2-450D14, (b) LGO@SiO_2-300D18, (c) LGO@SiO_2-150D20 (d) LGO@SiO_2-600D20.

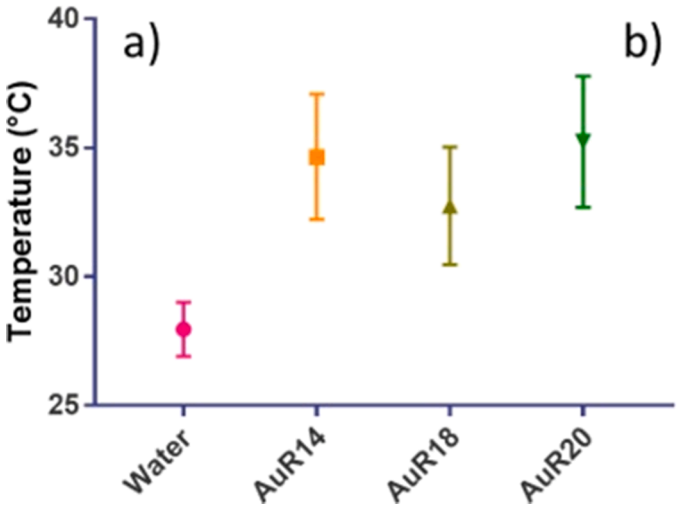

Sample	iT (°C)	fT (°C)	ΔT (°C)
Water	23.2	28.7	5.5
AuR14	24.3	36.2	11.9
AuR18	24.5	34.5	10.0
AuR20	24.1	36.8	12.7

Fig. 9. PPTT effect on AuR: (a) Change induced by the photothermal heating temperature values obtained after irradiating the AuR samples with an 808 nm wavelength laser for 30 min and 800 mW, (b) Comparisons between the initial (iT) and final temperatures (fT). The initial temperature was measured at room temperature.

presence of the LSPR. Four graphs, each with three absorbance spectra, are shown in Fig. 8. All black lines are associated with the LGO@SiO_2 and the functionalization of its surface with the MPTMS- AMPTMS. The black lines are used as control (stock solution). In all four spectra, a signal-centered peak is present at ~900 nm, which is associated to the coating with SiO_2 [21].

The four graphs display a red line, which corresponds to the absorbance spectra of the different AuR. Consequently, the red line in Fig. 8a corresponds to AuR14, while the red line in Fig. 8b is associated with AuR18, and the red line in Fig. 8c and d corresponds to AuR20. In all cases, the control sample shows the two typical absorbance bands of AuR (Fig. 4a).

In Fig. 8, the blue lines are associated with the absorbance of the hybrid materials. It is important to notice that all blue lines (absorbance bands) associated with LSPR are preserved. In addition, they present an attenuation in intensity compared to the LSPR bands corresponding to the AuR (red lines). In addition, the blue lines show a shift towards lower energy wavelengths. These phenomena are associated with an increase in the aspect ratio of the hybrid materials, which occurs when the AuR nanoparticles are anchored on the surface of the LGO@SiO_2 [22].

On the other hand, the absorbance spectrum of the hybrid materials shows a widening of the absorption band, which could be related to the extinction cross-section and electron mean free path in the AuR [23]. The UV-Vis characterization shows that the bands associated with characteristic LSPR of the AuR prevail in the hybrid materials. The significance of this point is due to the permanence of the absorbance bands. The activation of the LSPR could be allowed, which could induce a localized temperature increase and, therefore, be used as a possible therapeutic agent for the treatment of degenerative diseases such as cancer.

Physicochemical characterization confirmed that luminescence of LGO and LSPR of AuR were preserved in the hybrid materials.

Hybrid materials were further analyzed for the PPTT effect due to the LSPR. For this purpose, the hybrid materials were irradiated with a laser of 808 nm wavelength, which coincides with the resonant frequency of the localized surface plasmon of the hybrid materials. The first

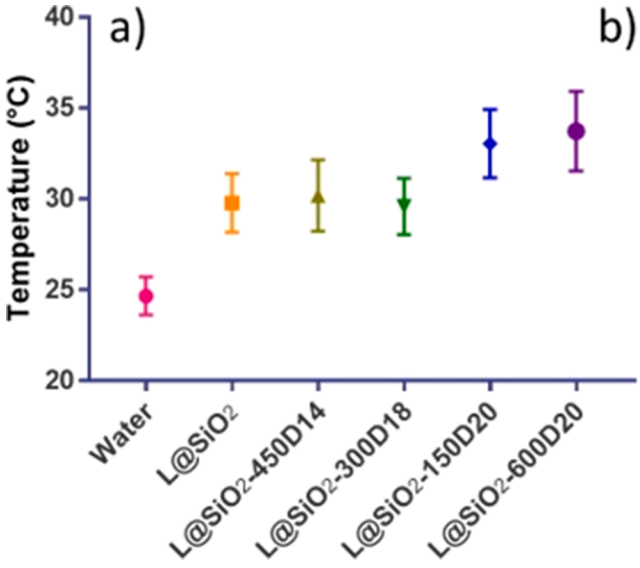

Sample	iT (°C)	fT (°C)	ΔT (°C)
Water	22.4	28.2	5.8
L@SiO_2	25.1	32.1	7.0
L@SiO_2-450D14	22.8	29.0	6.2
L@SiO_2-300D18	21.2	27.7	6.5
L@SiO_2-150D20	23.3	34.0	10.7
L@SiO_2-600D20	24.5	34.0	9.5

Fig. 10. PPTT effect on hybrid materials: Samples irradiated with a wavelength of 808 nm at 800 mW for 30 min, the initial temperature is equal at room temperature. (a) Change induced by photothermal heating temperature of the hybrid materials. (b) Comparisons between initial and end temperature, obtained after irradiating the hybrid materials.

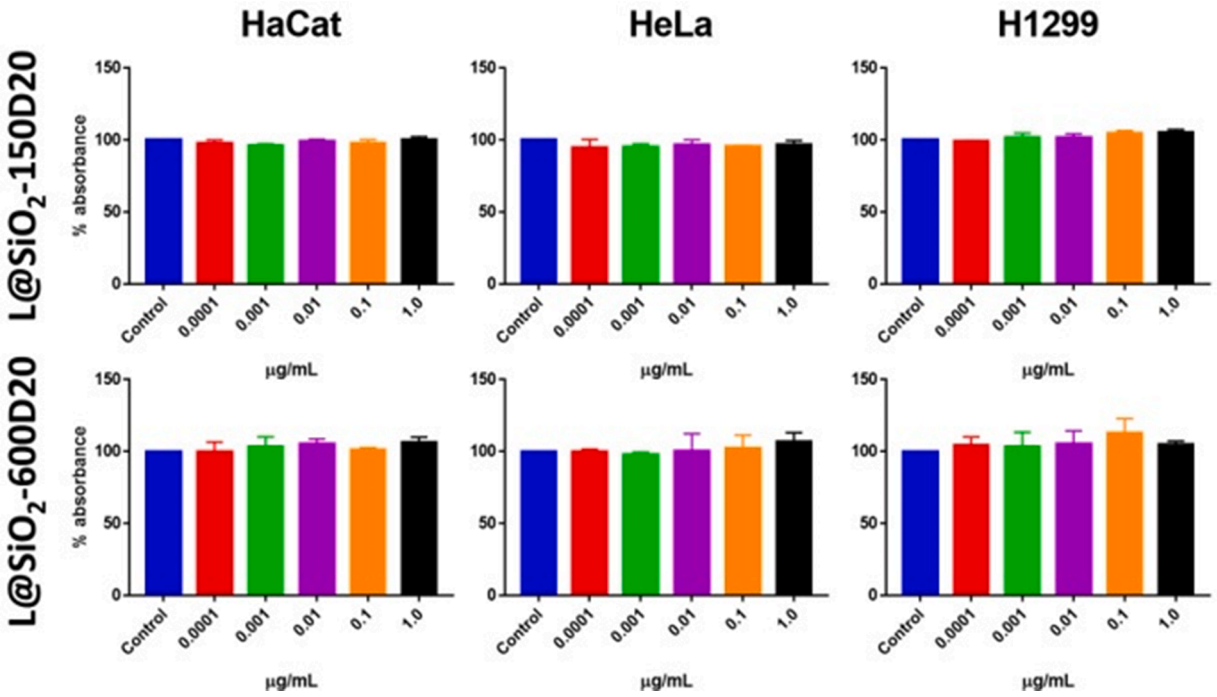

Fig. 11. Cell viability assay using hybrid materials: L@SiO_2-150D20 and L@SiO_2-600D20. Cell lines HaCat, HeLa, and NCI-H1299 were treated with different concentrations of hybrid materials and cell viability was assessed by the MTS assay after 24 h.

measurement was made by irradiating the three different AuR, used at a concentration of 1 mM CTAB. The samples were irradiated at a power of 800 mW for 30 min; water was used as control, and in Fig. 9 the initial temperature (iT) refers to the room temperature. The sample containing only deionized water showed a temperature increase of 5.5 °C (ΔT) (Fig. 9). AuR samples showed increases in temperature compared with the control, which were 11.9, 10 and 12.7 for AuR14, AuR18 and AuR20, respectively. The increase in temperature is due to the generation of heat associated with the photo-physical processes that occur as a response to the absorption of light. Firstly, the absorbed light energy is converted to heat to form a hot metallic lattice by two processes: electron-electron relaxation and electron-phonon relaxation. Hot electron temperatures are easily reached into the surface of the nanoparticles, and the lattice then cools off by a phonon-phonon relaxation process, by which the heat is dissipated via the particles to the surrounding environment, thereby causing localized heating [12]. The temperature increase values for the AuR matched the results reported by Mackey et al. [10].

The highest temperature increase was displayed by AuR20 due to its aspect ratio. It is generated from the outer part of the particles facing the incoming light. For elongated nanorods, the inner part of the particle gets closer to the surface part and no longer suffers from shielding effect, which explains the increase in the heating efficiency for AuR20 [24].

A second measurement was performed to detect the temperature rise of the hybrid materials after light irradiation. Two control samples were used in this measurement, water and the stock solution (LGO@SiO_2). The hybrid materials were irradiated for 30 min with the laser of 808 nm at 800 mW. Fig. 10 shows the results of temperature increments.

The difference in temperature effect between the two control samples is 1.2 °C. Therefore, where the sample related to the LGO@SiO_2 presents the highest increase in temperature, associated with the 808 nm irradiation, it could activate the vibrational frequencies of the LGO@-SiO_2 components with a subsequent dissipation of energy in the form of heat.

The sample that showed the greatest increase in temperature was L@SiO_2-150D20 with a ΔT=10.7 °C. However, the L@SiO_2-600D20 sample was expected to display a higher increase in temperature compared with the L@SiO_2-150D20 due to the presence of a higher amount of AuR20.

When analyzing the shift of the LSPR signals from hybrid materials (Fig. 8c and d), the peak associated with AuR20 is centered at ~777 nm. In comparison, this band is centered at ~810 nm for L@SiO_2-150D20 and at ~819 nm for L@SiO_2-600D20, which represents a shift concerning the AuR20 of 32 nm and 42 nm, respectively. A higher displacement towards the NIR of the surface plasmon band could be associated with the possible agglomeration of AuR on the LGO surface. This agglomeration could influence the interaction of the AuR with the incident light, a phenomenon that may explain the lower temperature increase presented by the L@SiO_2-600D20.

The hybrid materials synthesized from AuR14 and AuR18 presented an increase in temperature below that shown by the control samples. This can be attributed to a poor anchoring of AuR on luminescent materials.

According to the increase in temperature after irradiating the hybrid materials with infrared light, the hybrid materials synthesized from AuR20 were selected to evaluate their potential cytotoxic effect by assessing cell viability in three different cell lines: HaCaT (immortalized keratinocytes), HeLa (cervical cancer-derived cell line), and H1299 (lung cancer-derived cell line).

Cell proliferation was assayed as an initial approach to determine the effect of the hybrid materials on the metabolic activity of the different cell lines. This procedure was done by the MTS assay. Fig. 11 shows the results of the cell treatment with both selected hybrid materials. The data were processed by ANOVA, and no significant difference was found between control cells and cells exposed to different concentrations of the hybrid materials. These results indicate that the hybrid materials do not interfere with the metabolic activity of the cells.

The absence of the cytotoxic effects of the synthesized materials points to their potential use in future investigations, and the biocompatibility results presented here will allow testing of the hybrid materials in different *in vivo* models. Future investigations will need to determine the acceptance of these materials using biologically complex models, such as mice, and determine the ability of the materials to induce cell death of a specific type of cells.

Conclusion

The synthesis of hybrid materials formed by LGO and AuR was successfully achieved in this work. Characterization of the luminescent properties of the hybrid materials showed excellently preserved near infrared emission associated with the presence of LGO. Additionally, the properties of LSPR were maintained, associated with anchoring the AuR on the surface of phosphors.

As a first approach, the materials were irradiated with a wavelength of 808 nm for 30 min and power of 800 mW, to measure the responses of the hybrid materials and the temperature change in the medium. The results of this response are associated with the presence of the longitudinal plasmon band of AuR, which remains present in the hybrid materials producing a temperature increase.

Finally, in this work, the first cell viability assays of the hybrid materials are presented. The novel hybrid materials were tested on immortalized HaCaT cells, as well as on cancer-derived cell lines such as HeLa and H1299. The hybrid materials presented excellent biocompatibility in all assays. Additional studies are under progress in order to improve the synthesis conditions, such as increasing the AuR amount with less agglomeration, and at the same time enhancing the response to laser radiation towards a higher in temperatures of the hybrid nanocomposite materials.

CRediT authorship contribution statement

C. Belman-Rodriguez: Conceptualization, Investigation, Methodology, Validation, Writing – original draft. **Prakhar Sengar:** Writing – review & editing, Conceptualization. **Gustavo A. Hirata:** Writing – review & editing, Visualization. **Joaquin Manzo-Merino:** Resources, Investigation, Funding acquisition. **Marcela Lizano:** Resources. **Mario H. Farías:** Writing – review & editing. **Sergio A. Aguila:** Supervision, Project administration, Funding acquisition.

Declaration of Competing Interest

The authors declare that they have no known competing financial interests or personal relationships that could have appeared to influence the work reported in this paper.

Acknowledgments

The authors acknowledge financial support from DGAPA-UNAM under Grants Nos. IG200320 and IN-115520 and CONACyT under Grant No. 284548. We express our gratitude to Eloisa Aparicio (X-ray diffraction technician), Israel Gradilla (SEM technician), Francisco Ruiz (TEM technician), Jaime Mendoza (characterization analyzes), and to María Isabel Pérez Montfort who corrected the English version of the manuscript at CNyN, UNAM. C. Belman-Rodriguez thanks CONACyT for scholarship grant 333216.

References

[1] C. Iancu, Photothermal therapy of human cancers (PTT) using gold nanoparticles, Biotechnol. Mol. Biol. Nanomed. 1 (2013) 53–60, https://doi.org/10.1016/j.biomaterials.2011.08.086.

[2] S. Khizar, N.M. Ahmad, N. Zine, N. Jaffrezic-Renault, A. Errachid-El-Salhi, A. Elaissari, Magnetic nanoparticles: from synthesis to theranostic applications, ACS Appl. Nano Mater. 4 (2021) 4284–4306, https://doi.org/10.1021/acsanm.1c00852.

[3] Q. Wei, J. He, S. Wang, S. Hua, Y. Qi, F. Li, D. Ling, M. Zhou, Low-dose X-ray enhanced tumor accumulation of theranostic nanoparticles for high-performance bimodal imaging-guided photothermal therapy, J. Nanobiotechnol. 19 (2021) 1–17, https://doi.org/10.1186/s12951-021-00875-8.

[4] V.K.A. Sreenivasan, A.V Zvyagin, E.M. Goldys, Luminescent nanoparticles and their applications in the life sciences, J. Phys. Condens. Matter 25 (2013), 194101, https://doi.org/10.1088/0953-8984/25/19/194101.

[5] Z. Jun, X. Zhiguo, L. Xiong, Y. Xiangyan, S. Jiayue, X. Denghui, A novel near-infrared $LiGaW_2O_8$:Yb^3+,Cr^3+ up-conversion phosphor with enhanced luminescence intensity based on Ho^3+/Er^3+ bridges, J. Mater. Chem. C (2020) 10715–10722, https://doi.org/10.1039/D0TC02963G.

[6] E. Hemmer, N. Venkatachalam, H. Hyodo, A. Hattori, Y. Ebina, H. Kishimoto, K. Soga, Upconverting and NIR emitting rare earth based nanostructures for NIR-bioimaging, Nanoscale 5 (2013) 11339–11361, https://doi.org/10.1039/c3nr02286b.

[7] F. Liu, W. Yan, Y.J. Chuang, Z. Zhen, J. Xie, Z. Pan, Photostimulated near-infrared persistent luminescence as a new optical read-out from Cr^3+-doped $LiGa_5O_8$, Sci. Rep. 3 (2013) 1–9, https://doi.org/10.1038/srep01554.

[8] H. Chen, X. Sun, G.D. Wang, K. Nagata, Z. Hao, A. Wang, Z. Li, J. Xie, B. Shen, $LiGa_5O_8$:Cr-based theranostic nanoparticles for imaging-guided X-ray induced photodynamic therapy of deep-seated tumors, Mater. Horiz. 4 (2017) 1092–1101, https://doi.org/10.1039/c7mh00442g.

[9] O.Q. De Clercq, D. Poelman, Local, temperature-dependent trapping and detrapping in the $LiGa_5O_8$:Cr infrared emitting persistent phosphor, ECS J. Solid State Sci. Technol. 7 (2018) R3171–R3175, https://doi.org/10.1149/2.0211801jss.

[10] M.A. MacKey, M.R.K. Ali, L.A. Austin, R.D. Near, M.A. El-Sayed, The most effective gold nanorod size for plasmonic photothermal therapy: theory and *in vitro* experiments, J. Phys. Chem. B 118 (2014) 1319–1326, https://doi.org/10.1021/jp409298f.

[11] E.B. Dickerson, E.C. Dreaden, X. Huang, I.H. El-Sayed, H. Chu, S. Pushpanketh, J. F. McDonald, M.A. El-Sayed, Gold nanorod assisted near-infrared plasmonic photothermal therapy (PPTT) of squamous cell carcinoma in mice, Cancer Lett. 269 (2008) 57–66, https://doi.org/10.1016/j.canlet.2008.04.026.

[12] X. Huang, M.A. El-Sayed, Plasmonic photo-thermal therapy (PPTT), Alex. J. Med. 47 (2011) 1–9, https://doi.org/10.1016/j.ajme.2011.01.001.

[13] M.J. Sailor, J.H. Park, Hybrid nanoparticles for detection and treatment of cancer, Adv. Mater. 24 (2012) 3779–3802, https://doi.org/10.1002/adma.201200653.

[14] P. Sengar, K. García-Tapia, B. Can-Uc, K. Juárez-Moreno, O.E. Contreras-López, G. A. Hirata, Simultaneous paramagnetic and persistence-luminescence in GAGG:Ce, Pr nanoparticles synthesized by sol-gel for biomedical applications, J. Appl. Phys. (2019) 126, https://doi.org/10.1063/1.5098788.

[15] P. Sengar, G.A. Hirata, M.H. Farias, F. Castillón, Morphological optimization and (3-aminopropyl) trimethoxy silane surface modification of $Y_3Al_5O_{12}$: Pr nanoscintillator for biomedical applications, Mater. Res. Bull. 77 (2016) 236–242, https://doi.org/10.1016/j.materresbull.2016.01.045.

[16] B. Nikoobakht, M.A. El-Sayed, Preparation and growth mechanism of gold nanorods (NRs) using seed-mediated growth method, Chem. Mater. 15 (2003) 1957–1962, https://doi.org/10.1021/cm020732l.

[17] S.L. Westcott, S.J. Oldenburg, T.R. Lee, N.J. Halas, Formation and adsorption of clusters of gold nanoparticles onto functionalized silica nanoparticle surfaces, Langmuir 14 (1998) 5396–5401, https://doi.org/10.1021/la980380q.

[18] R.S. Riley, E.S. Day, Gold nanoparticle-mediated photothermal therapy: applications and opportunities for multimodal cancer treatment, Wiley Interdiscip. Rev. Nanomed. Nanobiotechnol. 9 (2017), https://doi.org/10.1002/wnan.1449.

[19] O.Q. De Clercq, L.I.D.J. Martin, K. Korthout, J. Kusakovskij, H. Vrielinck, D. Poelman, Probing the local structure of the near-infrared emitting persistent phosphor $LiGa_5O_8$:Cr^{3+}, J. Mater. Chem. C. 5 (2017) 10861–10868, https://doi.org/10.1039/C7TC02699D.

[20] J.Y. Kim, M.G. Han, M. Bin Lien, S. Magonov, Y. Zhu, H. George, T.B. Norris, N. A. Kotov, Dipole-like electrostatic asymmetry of gold nanorods, Sci. Adv. 4 (2018), https://doi.org/10.1126/sciadv.1700682.

[21] B. Pivac, P. Dubcek, J. Dasovic, H. Zorc, S. Bernstorff, J. Zavasnik, B. Vlahovic, Self-ordered voids formation in SiO_2 matrix by ge outdiffusion, J. Nanomater. (2018) 1–9, https://doi.org/10.1155/2018/9326408, 2018.

[22] X. Huang, I.H. El-Sayed, W. Qian, M.A. El-Sayed, Cancer cell imaging and photothermal therapy in the near-infrared region by using gold nanorods, J. Am. Chem. Soc. 128 (2006) 2115–2120, https://doi.org/10.1021/ja057254a.

[23] H.R. Nikabadi, N. Shahtahmasebi, M.R. Rokn-Abadi, M.M.B. Mohagheghi, E. K. Goharshadi, Gradual growth of gold nanoseeds on silica for SiO_2 @gold homogeneous nano core/shell applications by the chemical reduction method, Phys. Scr. 87 (2013) 2–7, https://doi.org/10.1088/0031-8949/87/02/025802.

[24] G. Baffou, R. Quidant, C. Girard, Heat generation in plasmonic nanostructures: Influence of morphology, Appl. Phys. Lett. 94 (2009), https://doi.org/10.1063/1.3116645.